Maximizing the Strength of Fused-Deposition ABS Plastic Parts

J. F. Rodríguez, J. P. Thomas, and J. E. Renaud
University of Notre Dame
Department of Aerospace and Mechanical Engineering
Notre Dame, IN 46556-5637
USA

ABSTRACT

Fused-Deposition (FD) creates parts using robotic extrusion of a semi-liquid polymer fiber, which molecularly bonds with neighboring fibers via thermal-diffusion bonding. The strength of the part depends on the bulk polymer strength, the mesostructure (fiber layout, void geometry, extent of fiber bonding), and the fiber-to-fiber bond strength. The influence of these factors on the mechanical strength of FD-ABS plastic parts is reported along with the FD process variable settings for maximum strength. Substantial increases in transverse strength are achieved at the optimal settings and additional increases can be achieved by post-fabrication annealing.

Keywords: Stratasys, fused-deposition, ABS plastic, functional parts, strength, mesostructure, polymer diffusion.

INTRODUCTION

Fused-Deposition (FD) Modeling is a Solid Freeform Fabrication (SFF) process that creates a physical representation of a CAD model via computer-controlled robotic extrusion of a small polymeric fiber in an additive material deposition process. The fibers are extruded in a semi-liquid state and bond with the neighboring fibers via thermal-diffusion welding. FD materials take the form of laminate composites with vertically stacked layers consisting of contiguous material "roads" or "fibers" with voids. The ability of FD create geometrically complex parts with specific mesostructural characteristics endow it with unique potential for the manufacture of functional parts with tailored mechanical performance. However, better understanding of the influence of the mesostructure and FD process variables on the mechanical behavior is needed to fully capitalize on this potential.

There have been several efforts to characterize and improve the mechanical behavior of FD materials. Fodran and coworkers [1998] studied the effect of impregnating the FD material with adhesive bonding agents after manufacturing to improve stiffness and strength. Kulkarni, et al. [1997] compared experimentally measured in-plane tensile moduli for symmetric FD composites built with various deposition strategies with predictions made using laminate composite theory. Gray et al. [1998] investigated the use of fiber reinforced polypropylene for making much stronger and stiffer FD parts. Bertoldi et al. [1998] characterized the elastic moduli for FD-ABS materials with a "pseudo-isotropic" stacking sequence.

This paper summarizes the results of various studies conducted at Notre Dame on the influence of mesostructure and FD processing parameters on the strength of unidirectional FD-ABS (acrylonitrile-butadiene-styrene) plastic materials. Our studies show that the strength and stiffness of FD parts is controlled by the bulk ABS material properties, void geometry, extent of bonding between contiguous fibers, and the strength of the fiber-to-fiber bonds. Decreasing the FD gap setting from 0.0 to $-25.4\,\mu m$ reduces the void size and increases the contact between contiguous fibers resulting in a significant increase in transverse strength. Increasing the FD envelope temperature and post-build annealing increases the strength of the bonds between the fibers, which also produces an increase in the transverse strength.

We start with a description of the experiments used to characterize the mesostructure, fiber-to-fiber bond strength, and material strengths as a function of the various FD processing parameters. The experimental results are presented and discussed, and the paper ends with conclusions and recommendations for future work.

METHOD

The Stratasys FDM1600 Modeler with the P400 ABS plastic was used to make the test specimens. The P400 ABS is supplied in monofilament form (1.778 mm diameter) and is kept in the shipping container or the FDM1600 material feed chamber with desiccant to minimize the absorption of humidity.

The FDM1600 has hardware and software based parameters that can influence the material strength. The fiber-to-fiber gap, g, (0 to $-50.4\mu m$) has a large influence on the extent of bonding between fibers within a given layer and on the resulting material density. The fiber cross-section geometry is controlled by the normalized flow rate, ϕ, (16-30$\equiv$nominal fiber width in mils), the layer height (0.254 mm), the nozzle diameter (0.308 mm), and the nozzle speed during extrusion (12.7 mm/sec). The fiber layout can be controlled within each layer (unidirectional, contour) and between each layer (translation: aligned or skewed; and rotation). The extrusion (~285°C max) and envelope temperatures (70°C max) influence the viscous flow and solidification characteristics and the thermal-diffusion bonding process between fibers. Parameter settings that minimize the void and defect densities and maximize the extent of fiber-to-fiber bonding produce FD materials with the maximum elastic strength and stiffness.

Only unidirectional FD materials with aligned (vertically aligned stacking; Figures 1,2) or skewed (alternating layers with horizontal skewing one-half the fiber width) mesostructures are considered in this paper. The void areal density and the extent of circumferential fiber-to-fiber bonding have been characterized as a function of fiber-to-fiber gap, flow rate (fiber width), and the extrusion and envelope temperatures. Void density on the i^{th} material plane is defined as:

$$\rho_i = \frac{Void\ Area}{Cross\ Section\ Area} \tag{1}$$

The extent of circumferential fiber-to-fiber bonding is quantified using the fiber interface bond length density:

$$B.L.\ Density = \frac{\sum Fiber\ Bond\ Lengths}{Total\ Circumference\ Length} \tag{2}$$

Mesostructure characterization was performed using cross-section micrographs (Rodriguez et al., 1997, 1999b). Void densities in the plane normal to the fiber extrusion direction were determined using a point counting method. Bond length densities were determined by subdividing fiber circumferences into arcs and summing the respective contributions. The reported densities are averages based on ten or more measurements.

The fiber-to-fiber bond strength was characterized in terms of interface fracture toughness (Rodriguez et al., 1999a). Tests were performed to assess the influence of the extrusion and envelope temperatures, loading rate, and post-build annealing treatments on the bond strength. The test specimens are sheet-like, one fiber thick, and have an edge crack at the interface between fibers (Figure 3).

The stress-strain behavior of bulk ABS monofilament and FD-ABS under longitudinal, transverse, and off-axis loading was determined under strain control. The test specimens (Figure 4) are in a tabbed-coupon configuration with dimensions conforming to ASTM Standard D3039.

RESULTS

The fiber gap and flow rate had a large influence on mesostructure while extrusion and envelope temperatures had very little influence. The lowest void densities (6.8%A, 4.5%S) and largest bond densities (73%A, 69%S) are achieved at the following settings: $g = -25.4\mu m$, $\phi = 20$, $T_L = 270°C$ and $T_E = 70°C$, henceforth denoted as "optimal." Photographs of an aligned mesostructure at gap settings of 0.0 and $-25.4\mu m$ are shown in Figures 1 and 2. For skewed mesostructures with positive gap, the maximum void density achieved was 16% at $g = 152\mu m$ with a corresponding bond-length density of 39%. The fiber cross-sections were asymmetrical, and the voids were either triangular or diamond shaped depending on the gap setting and the magnitude of the extrusion-envelope temperature difference, $T_L - T_E$.

Fiber bond strengths (i.e., fracture toughness, K_c) for the envelope temperatures $T_E = 50$, 60, and $70°C$ are plotted in Figure 5 as a function of extrusion temperature ($T_L = 255$, 270, and $285°C$). K_c increases with T_L and T_E, but the increase levels out with T_L at the machine default setting of $270°C$. The increase in K_c with T_E is similar for all T_L values amounting to $0.014 MPa\sqrt{m}/°C$. The effect of displacement rate (0.013 to $0.85 mm/sec$) on K_c is relatively small, only $-0.08 MPa\sqrt{m}$ per decade increase in the rate. The effect of annealing treatment (1 *min* to 8 *hr* at 118, 125, or $134°C$) is shown in Figure 6. K_c increases linearly with respect to $t^{1/4}$ for a given anneal temperature. The bond strength before annealing ($1.88 MPa\sqrt{m}$) corresponds to the value for specimens built with the optimal settings. It reaches a maximum of $2.48 MPa\sqrt{m}$ at the so-called recovery time, t_∞. The observed power-law form is consistent with molecular diffusion theories for strength development at A/A polymer interfaces (Rodriguez et al., 1999a).

The fracture morphology in the small region of stable crack growth that occurs prior to reaching the critical fracture load is most relevant to the mechanistic understanding of strength at the fiber interface. SEM fractographs of this region for specimens built with the optimal settings, with and without annealing (64 minutes at $134°C$), are shown in Figures 7 and 8. The annealed specimen (Figure 8) shows less fibrillation (i.e., tear ridges due to crazing and molecular pullout at the interfaces between the butadiene particles and acryonitrile-styrene matrix) and more chain scission than the unannealed specimen (Figure 7), due to increased molecular interpenetration that occurs with annealing. Defects (e.g., voids and microcracks) at the interface between the bonded fibers (Figure 9) also influence the interface bond strength.

The stress-strain responses for bulk ABS and FD-ABS specimens loaded in the longitudinal and transverse directions are shown in Figure 10. Strength values for these and other mesostructures are listed in Table 1. Stresses in the FD specimens are calculated using apparent cross-section areas that do not account for the void area. The bulk and longitudinal FD stress-strain responses are qualitatively similar, but the FD-ABS strength (i.e., the maximum stress attained) is lower than the bulk ABS strength by $6.8 MPa$ (22%). The transverse FD stress-strain behavior is more "brittle" in nature with much lower strength and strain-to-failure values. The change in behavior is indicative of the change in failure mode from ductile fracture of the extruded FD fibers, for longitudinal loading, to brittle fracture along the fiber interfaces for transverse loading.

Figure 11 shows the strength values plotted as a function of angle, from longitudinal at $\theta = 0°$ to transverse, at $\theta = 90°$. The quadratic strength theory of Azzi and Tsai (1965) for

laminate composites is used to characterize the strength, S_θ, as a function of θ:

$$\frac{1}{S_\theta} = \frac{\cos^4\theta}{S_0^2} + \left(\frac{1}{S_S^2} - \frac{1}{S_0^2}\right)\cos^2\theta\sin^2\theta + \frac{\sin^4\theta}{S_{90}^2} \tag{3}$$

The coefficient, S_S, is quantified using the tensile strength at 10° (Rodriguez, 1999).

Table 1: Bulk ABS and FD-ABS Strength and (Modulus) Values

Mesostructure	Longitudinal (*MPa*)	Transverse (*MPa*)
Bulk ABS	31.2 (2230)	n/a
Aligned, $g = 0.0\mu m$	21.5	<5
Aligned, $g = -25.4\mu m$	24.4 (1972)	13.4 (1762)
Aligned, $g = -25.4\mu m$, Annealed	22.9	18.5
Skewed, $g = -25.4\mu m$	21.6 (1986)	13.4 (1701)
Skewed, $g = 76.2\mu m$	17.9 (1807)	13.4 (1400)

Figure 12 shows the effect of strain rate on the stress-strain response. A rather drastic reduction in toughness (area under the stress-strain curve) occurs at the lowest strain rate; this strain rate effect is not observed with the bulk ABS specimens. The size of the overshoot at the maximum stress also decreases with strain rate and commences at a smaller level of strain.

DISCUSSION

The strength of the FD-ABS material is lower than the bulk ABS strength for all loading orientations. The presence of voids in the FD-ABS material decreases the amount of load carrying material. The voids cannot be eliminated because the viscosity of the ABS cannot be lowered enough by high temperature to fill the voids without inducing excessive thermal damage. In transverse loading, the sharp corners at the junction of neighboring fibers and the weaker fiber-to-fiber interface material due to incomplete "mixing" of the polymer molecules promotes craze nucleation and propagation further reducing the strength.

Rule-of-mixture relations can be used with good accuracy to predict the effective tensile modulus and strength of unidirectional composite materials. In the present case, the rule of mixtures estimates for longitudinal FD-ABS modulus and strength are off by –5.4% and –19% respectively. One reason for the underestimation of these values is a suspected difference in the modulus and strength of bulk ABS versus extruded FD-ABS fibers due to increased molecular alignment in the bulk ABS. Molecular alignment can be discerned using thermal shrinkage experiments (Fritch, 1980). The larger the shrinkage experienced by a specimen, the larger is the degree of molecular alignment in the shrinkage direction. Strength and elastic modulus increase with increasing alignment. If our suspicions are correct, the bulk ABS should show more shrinkage along the extrusion axis than the FD-ABS fibers.

Shrinkage experiments were conducted at Notre Dame on bulk ABS monofilament and extruded FD-ABS fibers. Four specimens of each, equal in length (102 mm), were held in an oven at $110°C$ ($T_g = 94°C$) for 6 hrs. After cooling, the % shrinkage in length, $(L/L_0 - 1)\times 100$, was measured. The monofilament shrank an average of 20% while the FD fiber shrank only 0.4% indicating a much larger degree of molecular orientation in the bulk ABS. These results are consistent with the underestimates produced by the rule-of-mixtures predictions.

Polymer chain diffusion theory (i.e., reptation theory) can be used to develop additional understanding of the influence of the processing temperatures on the fiber-to-fiber bond strengths. Wool and coworkers [1986,1989] have used reptation theory to develop various models for the strength of isothermally bonded symmetric A/A polymer interfaces. An expression for interface toughness, K_c, can be derived from this work assuming the bond strength is proportional to the monomer interpenetration depth across the interface:

$$\frac{K_c(t,T,M,p)}{K_\infty} = \frac{K_0(T)}{K_\infty} + \int \frac{d}{d\tau}\left[\left(\frac{\tau}{t_\infty(T,M,p)}\right)^{1/4}\right] d\tau \tag{4}$$

This integral is evaluated over the time t at which the interface temperature, T, is above the glass transition temperature, T_g. M is the molecular weight of the polymer; p is the pressure normal to the interface, $K_0(T)$ is the interface toughness due to surface wetting; and K_∞ is the maximum attainable toughness (i.e., K_c for the virgin material). The time to reach K_∞ is known as the recovery time, $t_\infty(T,M,p)$, and is defined by:

$$t_\infty = C(M,p)\exp\left(Q_d/RT\right) \tag{5}$$

where C is the pre-exponential frequency factor; Q_d is the activation energy; and R is the universal gas constant ($8.314\ J/mol \cdot K$).

Based on Eqs. (4) and (5), one expects higher processing temperatures to produce diffusion-related increases in K_c due to the increase in time that the interface temperature is above T_g and the decrease in the recovery time at higher temperatures. Figure 5 shows this is true for increasing T_E and for increasing T_L between 255 and $270°C$. The increase in K_c with annealing time/temperature and K_c's conformance to the $t^{1/4}$ relationship (Figure 6) further support the applicability of Eqs. (4) and (5) to FD thermal-diffusion bonding process.

A transient heat transfer analysis of the FD thermal bonding process was conducted using the finite element method (Rodriguez et al., 1999a). The predicted interface temperatures, $T(t)$, were combined with C and Q_d estimates from Figure 6 to calculate the effect of different T_L and T_E combinations on the diffusion related contribution to bond strength (i.e., Eq. (4)). The diffusion contribution to K_c was consistently overpredicted, particularly as $T_L \rightarrow 285°C$. Two reasons for the overprediction are suspected. First, the activation energy calculated from Figure 6 (i.e., $390kJ/mol$) is strictly valid only at the lower temperatures used in the annealing treatment. At the higher extrusion temperatures, Q_d is expected to decrease, which will (significantly) lower the integral contribution in Eq. (4) due to the exponential nature of t_∞. The second factor is related to the degradation of ABS by molecular chain breaking, oxidation, and butadiene particle coelescence at the high temperatures used during FD extrusion (Casale et al., 1975; Kelleher, 1966). This temperature related degradation is being confirmed via comparison of the molecular weights and microstructures (i.e., the butadiene particle size distribution) of the bulk ABS with extruded FD-ABS. Introduction of inert gas atmosphere in the FD build envelope is also being considered as a means of preventing polymer oxidation damage.

Annealing produced a 38% increase in transverse strength and a 6.7% decrease in longitudinal strength consistent with increased molecular interpenetration at the interface and decreased polymer chain alignment via thermal randomization. Unfortunately, the annealing also leads to part distortion, which limits its usefulness as a strengthening method. Efforts are underway to devise an annealing schedule that minimizes distortion effects.

CONCLUSIONS

The results illustrate the two links between the mechanical behavior of FD-ABS materials and the FD process variables; namely, mesostructure and fiber-to-fiber bond strength. The strongest and stiffest unidirectional FD-ABS parts are obtained at the "optimal" parameter settings: $g = -25.4\mu m$, $\phi = 20$, $T_L = 270°C$, and $T_E = 70°C$. Advances in FD technology that will lead to improved mechanical performance of FD-ABS parts include: higher envelope temperatures (available on the newer Stratasys FDM models); ABS blends with a larger range of molecular chain lengths to increase the bond strength; and second-phase additions to the ABS (e.g., free and grafted nanotubes) to increase the FD-ABS fiber strength and the fiber-to-fiber interface strength.

REFERENCES

Azzi, V. D., and Tsai, S. W., 1965, *Experimental Mechanics*, Vol. 5, pp. 283-288.

Bertoldi, M., Yardimci, M. A., Pistor, C. M., Guceri, S. I., and Sala, G., 1998, *SFF Symposium Proc.*, Austin, TX, pp. 549-556.

Brown, N., 1986, "Yield Behavior of Polymers", *Failure of Plastics*, Oxford, NY, pp. 98-118.

Casale, A., Salvatore, O., and Pizzigono, G., 1975, *Polymer Engr. Sci.*, Vol. 15, pp. 286-293.

Fodran E., Koch M., and Menon, U., 1996, *SFF Symposium Proc.*, Austin, TX, pp. 419-442.

Fritch, L. W., 1980, PACTEC V Conference of the Society of Plastic Engineers, Los Angeles, CA, Vol. 1, Feb. 1980, pp. 184-216.

Gray, R. W., Baird, D. G., and Bøhn, D. G., 1998, *Rapid Prototyping Journal*, Vol. 4, pp. 14-25.

Kelleher, P. G., 1966, *J. Applied Polymer Science*, Vol. 10, pp. 843-857.

Kulkarni, P., and Dutta, D., 1997, Paper #DAC3987, *Proc. ASME Design Engr. Conf.*, ASME, Sacramento, CA.

Rodríguez, J. F., 1999, "Modeling the Mechanical Behavior of Fused Deposition Acrylonitrile-Butadiene-Styrene Polymer Components", Doctoral Dissertation, University of Notre Dame, Aerospace & Mechanical Engineering Department, Notre Dame, IN.

Rodríguez, J. F., Thomas, J. P., and Renaud, J. E., 1999a, "Tailoring the Mechanical Properties of Fused-Deposition Manufactured Components", *Proc. Rapid Prototyping and Manufacturing Conf.*, SME, Dearborn, MI, pp.

Rodríguez, J. F., Thomas, J. P., and Renaud, J. E., 1999b, "Characterization of the Mesostructure of Fused Deposition ABS Plastic Materials", *Rapid Prototyping Journal*, in review.

Rodríguez, J. F., Thomas, J. P., and Renaud, J. E., 1997, *CAE and Intelligent Processing of Polymeric Materials*, MD-Vol. 79, ASME, NY, pp. 299-308.

Wool, R. P., and O'Connor, K. M., 1981, *Journal of Applied Physics*, Vol. 52, pp. 5953-5963.

Wool, R. P., Yuan, B.-L., and McGarel, O. J., 1989, *Polymer Engineering and Science*, Vol. 29, pp. 1340-1367.

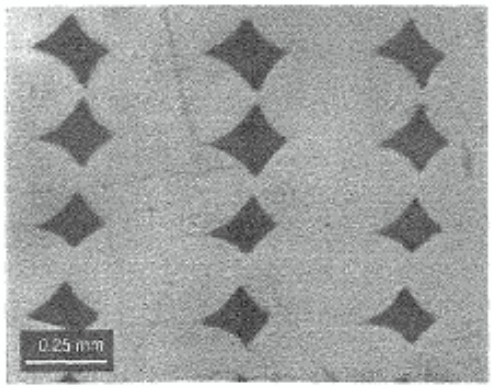

Figure 1: Mesostructure for the FD machine "default" settings: $g = 0.0\mu m$, $\phi = 20$, $T_L = 270°C$, and $T_E = 70°C$.

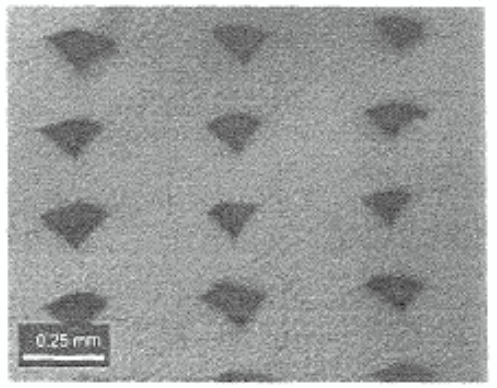

Figure 2: Mesostructure for the "optimal" FD machine settings: $g = -25.4\mu m$, $\phi = 20$, $T_L = 270°C$, and $T_E = 70°C$.

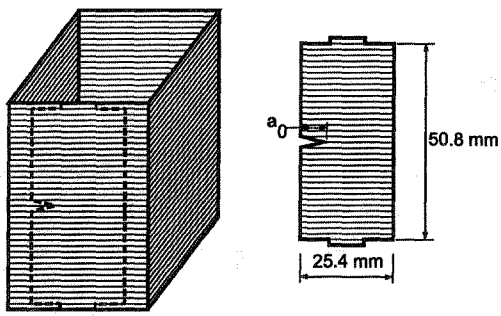

Figure 3: Fiber bond strength test specimen.

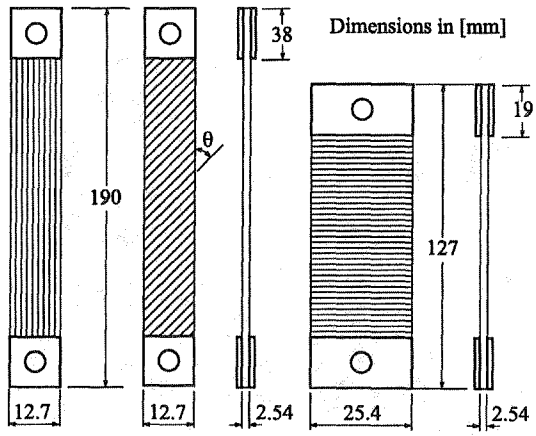

Figure 4: Tensile specimen geometries for longitudinal, off-axis, and transverse loading.

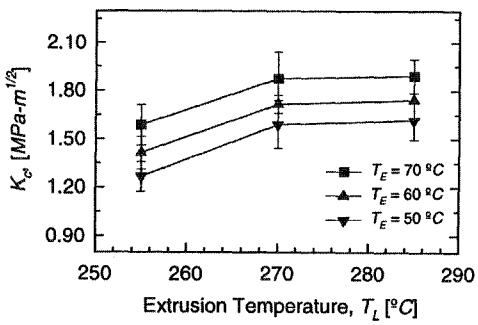

Figure 5: Fiber bond strength versus extrusion temperature for various envelope temperatures.

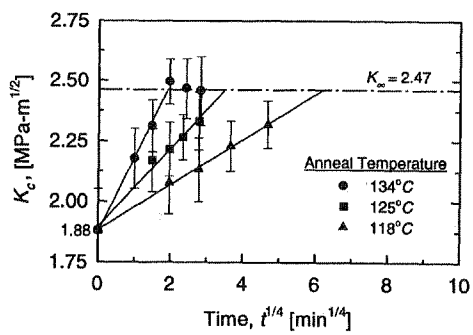

Figure 6: Fiber bond strength versus annealing time showing agreement with Equation (4).

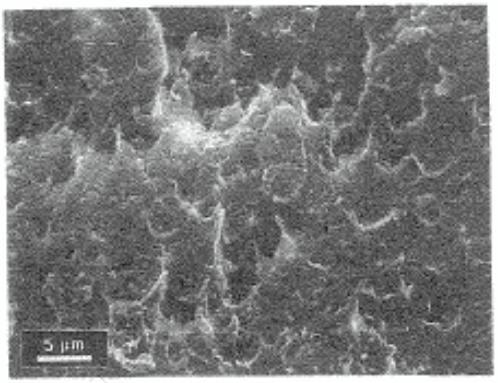

Figure 7: The fracture morphology in the stable crack growth region for a specimen built at the "optimal" machine settings, no annealing.

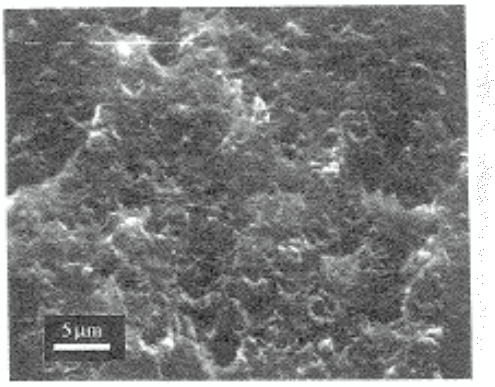

Figure 8: The fracture morphology in the stable crack growth region for a specimen built at the "optimal" machine settings and annealed at 134°C for 64 minutes.

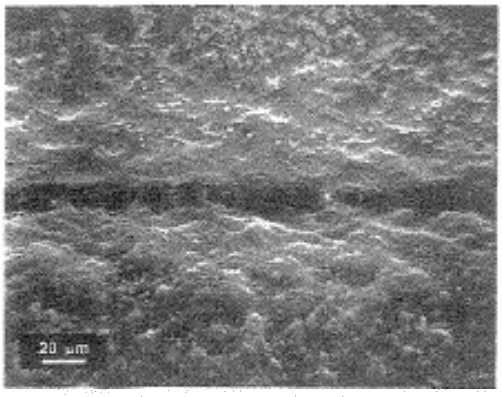

Figure 9: Interface zone between fibers showing typical void and microcrack defects.

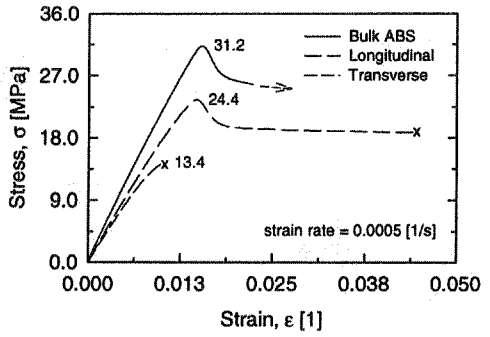

Figure 10: Stress-strain behaviors for the bulk ABS and FD-ABS built at the "optimal" FD machine settings.

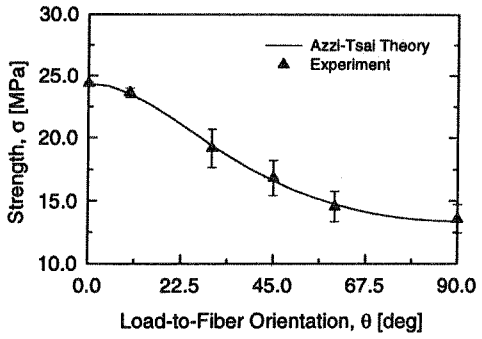

Figure 11: Experimental and predicted tensile strengths versus load-to-fiber orientation.

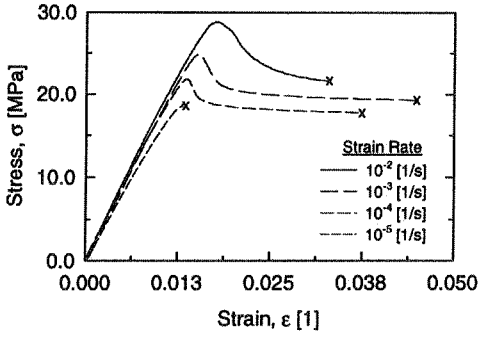

Figure 12: Influence of strain rate on the stress-strain behavior for longitudinal loading.